

Cite this article as: Du Suigeng, Li Na, Wang Songlin. Intermediate Phases of TiAl/GH3039 Friction Welding Joint[J]. Rare Metal Materials and Engineering, 2021, 50(09): 3102-3109.

ARTICLE

Intermediate Phases of TiAl/GH3039 Friction Welding Joint

Du Suigeng¹, Li Na^{1,2}, Wang Songlin¹

¹Key Laboratory of High Performance Manufacturing for Aero Engine, Ministry of Industry and Information Technology, Northwestern Polytechnical University, Xi'an 710072, China; ²Department of Mechanical and Electrical Engineering, Pingliang Vocational and Technical College, Pingliang 744000, China

Abstract: GH3039 superalloy was used as the third body metal to weld γ -TiAl with carbon steel, and the interface structure of the TiAl/GH3039 friction welding joint was analyzed by scanning electron microscope (SEM) and transmission electron microscope (TEM). The results show that the maximum tensile strength of the weld joint is more than 400 MPa after friction welding of γ -TiAl and GH3039 alloys. The plastic deformation of thermo-mechanically affected zone (TMAZ) on GH3039 side is larger than that on TiAl side, and dynamic recrystallization occurs on both sides. The Ni and Ti contents in the phase layer close to GH3039 and TiAl alloys hardly change, respectively. In the welding zone near GH3039 side, the distribution of Ni-rich and Cr-rich grains are complementary. Ti and Al are easily soluble in the Ni-rich crystal grains, and Mn is easily soluble in the Cr-rich crystal grains. A large number of Cr-rich grains formed in the bonding zone have body-centered cubic structure of α -Cr. The interface microstructure of the friction welding zone between γ -TiAl and GH3039 alloys is γ -TiAl/ α_2 -Ti₃Al/ α_2 + τ_3 / τ_3 -Al_{1+x-y}Ti_{1+y}Ni_{1-x}/ τ_3 + α -Cr/(Ni, Cr)_{ss}/GH3039.

Key words: friction welding; TiAl intermetallic; GH3039 superalloy; joint mechanism; interface microstructure

Conventionally, superalloy K418 and Inconel 713 are used as turbo of turbochargers. The rotor shaft of turbocharger is commonly made of AISI 4140 carbon steel. But the disadvantage of superalloy turbine is the large size, which results in a large mass of turbine rotor, a large moment of inertia, a poor transient response of the engine, and a large power loss. According to previous studies of the friction welding joint between K418 turbine disc and AISI 4140 shaft^[1], it is found that because of the difference between the physical and chemical performances of the welded materials, the friction interface is transformed and forms a "secondary" friction interface. The carbon is enriched at the secondary friction interface at high temperature, which results in the lower stress destruction of welding joint.

Meanwhile, TiAl intermetallic has small density, high elasticity modulus, and good high temperature performance. Therefore, TiAl alloy is regarded as the preferred material to replace superalloy in turbine manufacturing^[2-5]. In recent years, many kinds of welding methods have been used to study the connection of TiAl alloy. Many researches on TiAl brazing have been made and achieved great results^[6-11]. Li et

al^[12] studied vacuum brazing between TiAl and 42CrMo steel, and found that the tensile strength and shear strength of the joint are 347 and 229 MPa, respectively, after brazing at 900 °C for 5 min. Sequeiros et al^[13] joined γ -TiAl alloy with Inconel 718 by active metal brazing, using Incusil-ABA as filler, and found that the reaction between the base materials and the braze alloy produces multi-layered interfaces.

Electron beam welding is also widely used in TiAl connection^[14,15]. Li et al^[16] studied the microstructure of Ti-45Al-8.5Nb-0.2W-0.03Y joints after electron beam welding and found that crack-free welds can be achieved with pre-heating and post-heating treatments.

Diffusion welding, as an advanced welding method, has been applied to TiAl alloy connection^[17,18]. Zhao et al^[19] discussed the spark plasma sintering as a new method for diffusion bonding of TiAl alloys. It is found that the tensile strength of specimens depends on the percentage of metallurgical bonding and the interfacial microstructure, which can exceed the strength of base material under specific condition. Du et al^[20] conducted vacuum diffusion bonding on as-extruded Ti-47.5Al-Cr-V (at%) alloy. The results show that

Received date: September 07, 2020

Foundation item: National Natural Science Foundation of China (51675434)

Corresponding author: Du Suigeng, Ph. D., Professor, Key Laboratory of High Performance Manufacturing for Aero Engine, Ministry of Industry and Information Technology, Northwestern Polytechnical University, Xi'an 710072, P. R. China, Tel: 0086-29-88495264, E-mail: fwcenter@nwpu.edu.cn

Copyright © 2021, Northwest Institute for Nonferrous Metal Research. Published by Science Press. All rights reserved.

the shear strength and bonding interface quality of joints are increased with increasing the related bonding parameters.

Cai et al.^[21,22] welded TiAl alloy by laser welding, and found that TiAl alloy and Ni-based superalloy can be welded through V/Cu composite interlayer. The results indicate that insertion of V/Cu composite interlayer is very useful for laser welding of TiAl/Ni-based superalloy.

Friction welding is a pressure welding method. The welding workpiece can produce mechanical friction movement and generate heat between the contact surfaces of the welding materials, which makes the materials reach the thermoplastic state and then bend quickly to complete the welding. The future green welding technology has great technical potential and broad application prospect. Friction welding technique has already been applied to TiAl connection^[23-25]. Dong et al.^[26,27] discussed the effect of post-weld heat treatment on the microstructure and mechanical properties of friction welded joints of TiAl with 40Cr and 42CrMo alloys. Kumar^[28] investigated the friction welding characteristics between Ti-6Al-4V and SS304L alloys, and found that the highest tensile strength is acquired when pure copper is used as insert metal.

The existing studies indicate that it is very difficult to get excellent joint properties through direct friction welding of TiAl and AISI 4140 alloys, at the interface of which TiFe₂, TiAl, and TiC phases are formed. Therefore, the intermediate metal layer is necessary. AISI 4140 and TiAl alloys should be welded to an intermediate metal before the welding of target materials. GH3039 superalloy has high temperature performances which match well with those of TiAl, and better friction welding performance with carbon steel. GH3039 alloy is an ideal intermediate metal to achieve friction welding between TiAl and AISI 4140 alloys. However, the author's previous research^[29] shows that many brittle alloy phases are formed at the interface of TiAl and GH3039 friction welded joint, resulting in the decreased joint strength and poor plasticity. In order to improve the performance of TiAl and GH3039 friction welded joints and to understand the connection mechanism, it is necessary to investigate the interface structure. This research investigated the structure of interface between TiAl and GH3039 friction welded joints, laid a foundation for the practical application of TiAl in the field of turbocharger, and revealed the friction welding mechanism of intermetallic compounds and metals.

1 Experiment

The base alloy materials were TiAl alloy of $\Phi 25$ mm and GH3039 alloy. The chemical composition is listed in Table 1.

C500 type continuous drive friction welding machine equipped with industrial control computer with closed-loop control system was used, which could realize real-time

Table 1 Chemical composition of base alloys (wt%)

| Alloy | Al | Cr | V | Ti | Mo | Nb | Ni |
|--------|------|------|-----|------|-----|-----|------|
| TiAl | 47.5 | 1.0 | 2.5 | Bal. | - | - | - |
| GH3039 | 1.5 | 22.5 | - | 0.6 | 1.2 | 0.7 | Bal. |

detection and display and control the welding process parameters (welding pressure, axial speed, torque, and axial shortening). The welding parameters used in this study are listed in Table 2. Heat treatment was conducted after welding (560 °C/air cooling).

The tension strength of the welded joints was tested by DDL300 universal electric testing machine at loading speed of 1 mm/min. Quanta 400F field emission scanning electron microscope (FE-SEM) under backscattered electron (BSE) mode coupled with energy dispersive X-ray spectroscopy (EDS), Oxford INCA alpha-ray spectrometer, JEM-2100F transmission electron microscope (TEM), and JEOL-8230 electron probe were used to analyze the microstructure and fracture morphology of weld interface. The mechanism of friction welding of dissimilar materials was discussed and the structure of weld interface was investigated.

2 Results and Discussion

2.1 Macroscopic analysis of joint morphology

The appearance of welded joint after friction welding is shown in Fig. 1. It can be found that almost no macroscopic plastic deformation is formed on TiAl side, while on the GH3039 alloy side, the deformation is significant and unilateral burn-off is formed. This is because the high temperature strength of TiAl is far greater than that of GH3039 alloy. When the weld temperature increases to the temperature of thermal plastic stage of GH3039 alloy, TiAl can still maintain considerable high temperature strength. Also, TiAl has cast structure and plastic deformation barely occurs. Under the welding pressure, the plastic deformation on GH3039 side is enhanced. Under the constraint force, the unilateral burn-off forms with the bending.

Table 2 Welding parameters of process

| Parameter | Value |
|--------------------------------------------|-------|
| Initial rotating speed/r·min ⁻¹ | 1000 |
| Friction pressure/MPa | 8 |
| Forge pressure/MPa | 11 |
| Welding time/s | 8 |

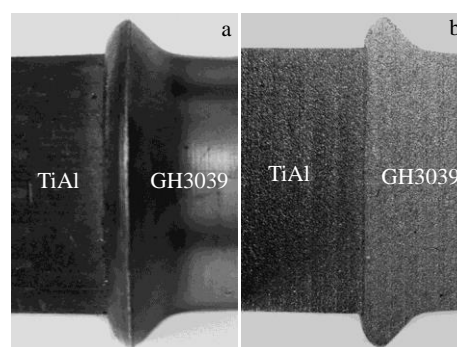


Fig.1 Appearance (a) and axial profile (b) of TiAl and GH3039 friction welded joint

Tensile properties of the welded parts were tested after welding. The results show that the maximum tensile strength of TiAl and GH3039 weldment reaches more than 400 MPa and most specimens fracture from TiAl base metal. It is shown that the strength of welded joint is greater than that of TiAl base metal. The fracture morphologies are shown in Fig. 2. According to Fig. 2a, the fracture is irregular and shows no trace of plastic deformation. It is clearly shown that the crack origin region stretches as a radial shape with slight river pattern. A small number of white γ -TiAl grains are found in the lamellar structure. The fracture plane is perpendicular to the direction of maximum pulling stress. The specimens of welded joints with lower tensile strength all fracture at the weld interface, as shown in Fig. 2b. The fracture surface is smooth, and the concentric circles formed by rotating friction can be found on the welding surface. It is also shown that some brittle alloy phases are formed on the welding surface. There is a small amount of TiAl base material adhering to GH3039 alloy on the right side of the fracture surface, which is in the near weld zone (WZ) of TiAl, and the fracture surface fluctuates greatly.

2.2 Microstructure analysis of joint morphology

After cutting the fracture specimen along the white line in Fig. 2b by wire electrical discharge machining (WEDM), WZ microstructure and the crack orientation can be observed completely. The WZ microstructure was analyzed by SEM with BSE image, as shown in Fig. 3. According to Fig. 3, there are four continuous intermediate phase layers formed at WZ, namely intermediate phase zone (IPZ). WZ includes IPZ and element diffusion zone on both sides. From GH3039 alloy side to TiAl base metal, the four continuous intermediate phase layers are denoted as A, B, C, and D in Fig. 3. The secondary cracks are mainly propagated between C and D intermediate phase layers and inside of the C intermediate phase layer, so the fracture performance of C intermediate phase layer is the worst. Near the GH3039 alloy, A and B intermediate phase layers are light gray phases and diffused on gray-white substrates. The gray phase in A and B intermediate phase layers is granular and flocculent, respectively. Both layers have abundant Cr element. The dark grey phases are C and D intermediate phase layers near the

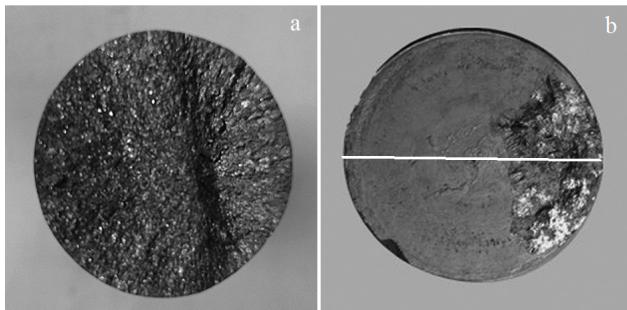


Fig.2 Fracture morphologies of friction welded joints at TiAl based metal side (a) and at weld seam (b)

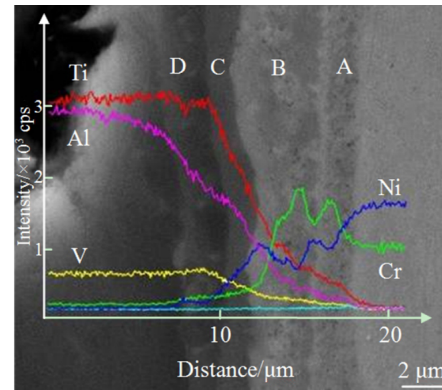


Fig.3 SEM-BSE image and EDS line scanning result of weld interface

TiAl side. Their color is similar to that of TiAl substrate. The only difference is that in D intermediate phase layer, a small number of white particles are dispersed.

The element distribution of the weld interface from the bottom GH3039 alloy to the upper TiAl base metal was determined by linear scanning of EDS with scanning length of about 8 μm , as shown in Fig. 3. The results show that the contents of Ti, Al, Ni, Cr, and V change greatly. It can be seen from Fig. 3 that the width of WZ is 4~5 μm . In intermediate phase layer A, the contents of alloy elements change significantly. On GH3039 side, the content of the main element Ni constantly decreases, while the content of Cr increases firstly and then decreases, indicating that the Cr-rich second phase is formed in IPZ. In intermediate phase layer D, there is a plain area where Ti and V are the main elements. The content of Al decreases significantly in this area, which means that a new phase is formed at this position and the diffusion rate of Al is faster than that of Ti. Different elements have different spread distances, thus forming different phase layers. The contents of Ni and Cr in intermediate phase layers A and B near GH3039 side are large, and the contents of Ti and Al in intermediate phase layers C and D near TiAl side are large.

In order to determine the distribution of each element in WZ, electron probe micro-analyzer (EPMA) was used to conduct the surface scanning test and the results are shown in Fig. 4.

It can be seen from Fig. 4a that the welded joint of TiAl and GH3039 alloys have four continuous phase layers formed in WZ as well (corresponding to A, B, C, and D intermediate phase layers in Fig. 3). After post-weld heat treatment, the four phase layers are clearly defined, and the internal composition of the phase layer is relatively uniform. However, the phase layer interface is not completely parallel with the weld seam, i. e., the width of phase layer at different positions of WZ is different. Since the activity and diffusion degrees of each element in the welding process are different, when the element concentration reaches a critical value, different intermetallic compound phase layers are generated. According to Ni

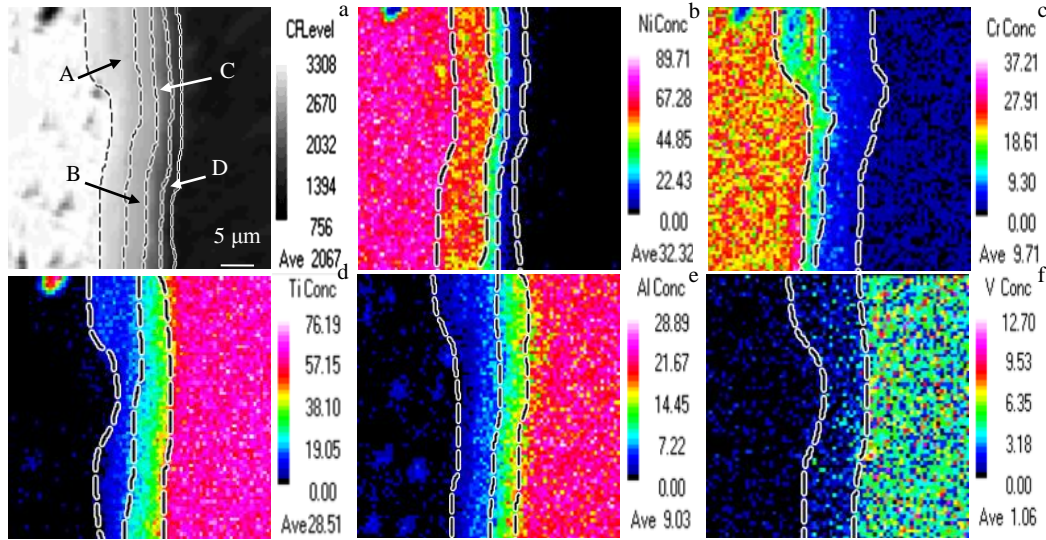


Fig.4 SEM-BSE image (a) and element distributions of Ni (b), Cr (c), Ti (d), Al (e), and V (f) of weld interface

element distribution in Fig. 4b, three different layers can be observed corresponding to the intermediate phase layers A, B, and C respectively. The Ni content in each intermediate phase layer does not change much, but it decreases orderly according to the distance between the intermediate phase layers and parent metal. Cr contents in intermediate phase layers A and B are higher than those in intermediate phase layers C and D. The element contents in intermediate phase layers A and B are obviously uneven. Ti content does not show significant decrease in intermediate phase layer D, compared with that in parent metal, and then decreases from intermediate phase layer C to B. There is still a certain amount of Ti in intermediate phase layer A, indicating that Ti element is diffused to the thermal mechanical affected zone (TMAZ) of GH3039 alloy, and the entire WZ has Ti element of different concentrations. Al element begins to decrease from intermediate phase layer D to A, remaining a certain amount in intermediate phase layer A, indicating that Al is also diffused to TMAZ on GH3039 side. V element has no significant decrease in intermediate phase layer D, compared

with that in base material, and gradually decreases in the other three intermediate phase layers. It can be seen from the analysis that the diffusion distances of Al and Ti are greater than those of Cr and Ni, and Al and Ti can diffuse into TMAZ of GH3039 alloy, while Cr and Ni can only diffuse into intermediate phase layer C. The contents of Ti and V in intermediate phase layer D hardly change.

In order to further explore the interface microstructure of WZ, TEM was used to observe the WZ. Fig. 5 shows the bright field TEM images of WZ. The boundaries (dotted line) between the TMAZ and WZ on TiAl and GH3039 sides can be seen clearly in Fig. 5a and 5b, respectively. It can be seen that grain sizes near WZ boundary are smaller than the sizes of grains after TMAZ recrystallization.

In order to show the element distributions in the WZ, the scanning transmission electron microscopy (STEM) was used to scan different zones. The EDS analysis results of the zone near IPZ lines on TiAl and GH3039 sides are shown in Fig. 6 and Fig. 7, respectively. The EDS analysis results of IPZ are shown in Fig. 8.

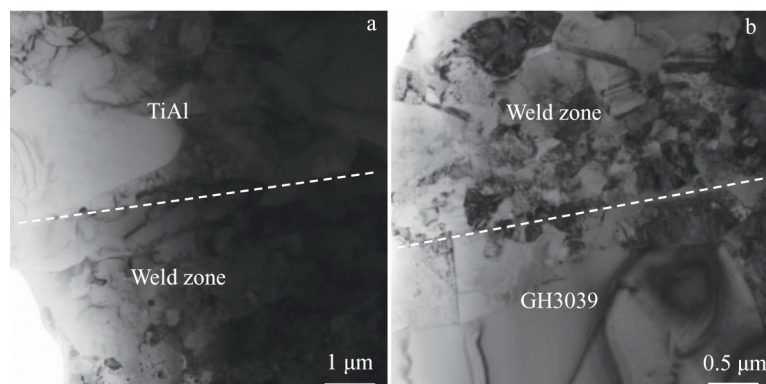


Fig.5 Bright field TEM images of boundaries between TMAZ and WZ on TiAl (a) and GH3039 (b) sides

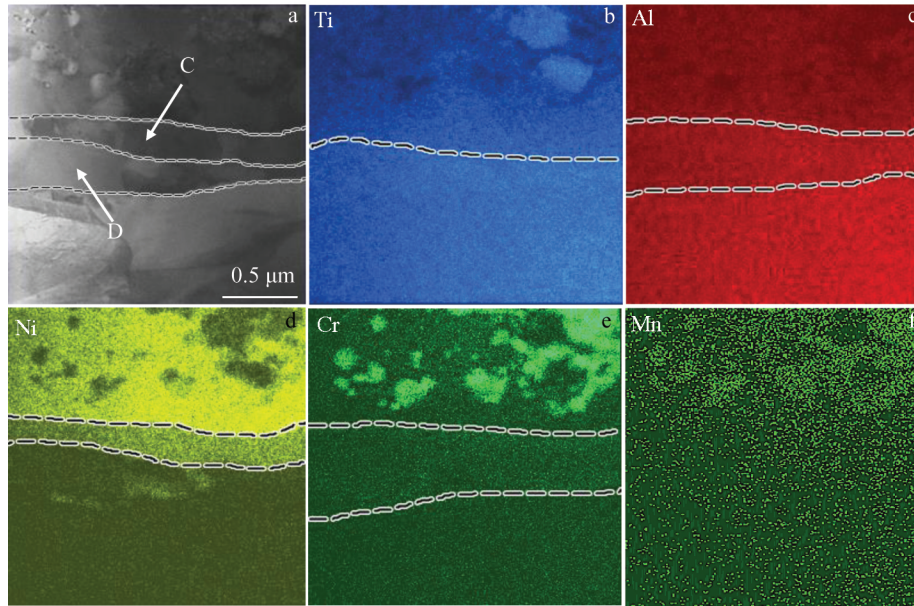


Fig.6 STEM image (a) and EDS mapping of Ti (b), Al (c), Ni (d), Cr (e), and Mn (f) element of zone near IPZ of TiAl side

The element distribution near the interface of TiAl WZ is clearly shown in Fig. 6. The C and D layers in Fig. 6a correspond to the intermediate phase layers C and D in Fig. 4, respectively. From TMAZ to WZ on TiAl side, the large elongated grains are transformed into fine recrystallized equiaxed grains, as shown in Fig. 6a. Ti and Al elements are evenly distributed in C and D layers. Ni is only diffused into C layer, while Cr does not enter C layer. The distribution of Ni, Cr, and Ti in IPZ (intermediate phase layer B) far from TiAl base metal is not uniform but complementary.

It can be seen from Fig. 7 that from TMAZ to WZ of

GH3039 side, the grain changes from large recrystallized grain to small equiaxed grain, and finally into equiaxed grain chunk of abundant Ni or Cr. The distribution of Ni-rich and Cr-rich grains is complementary, as shown in Fig. 7d and 7e. The Ti content in Ni-rich grains is high, as shown in Fig. 7b and 7d, and the S content in Cr-rich grains is high, as shown in Fig. 7e and 7f. According to the micro zone analysis, it can be determined that layer A is Ni based solid solution phase. The equiaxed grains of rich Cr in layer B are formed by precipitation in the base material and the spinodal decomposition under the thermo-mechanical coupling during welding.

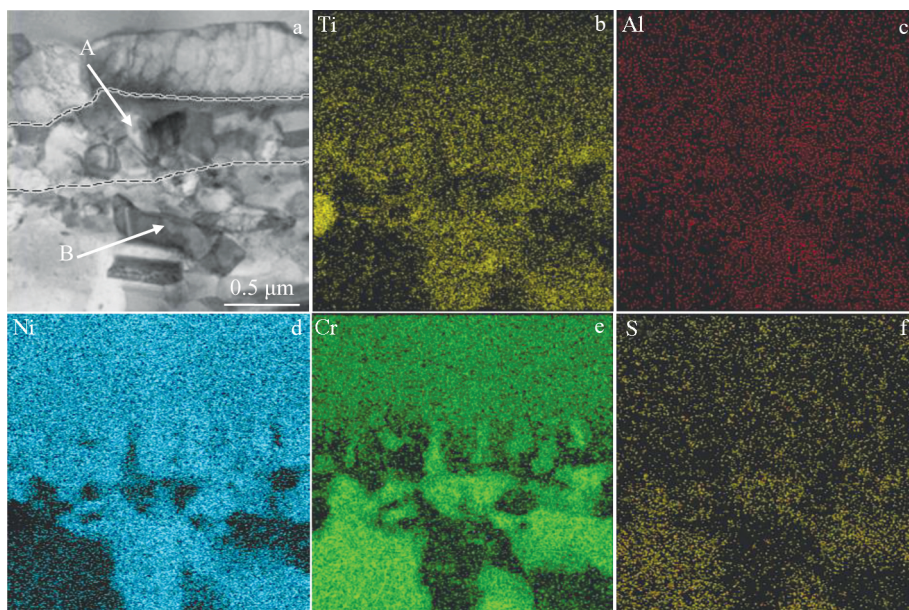


Fig.7 STEM image (a) and EDS mapping of Ti (b), Al (c), Ni (d), Cr (e), and S (f) element of zone near IPZ of GH3039 side

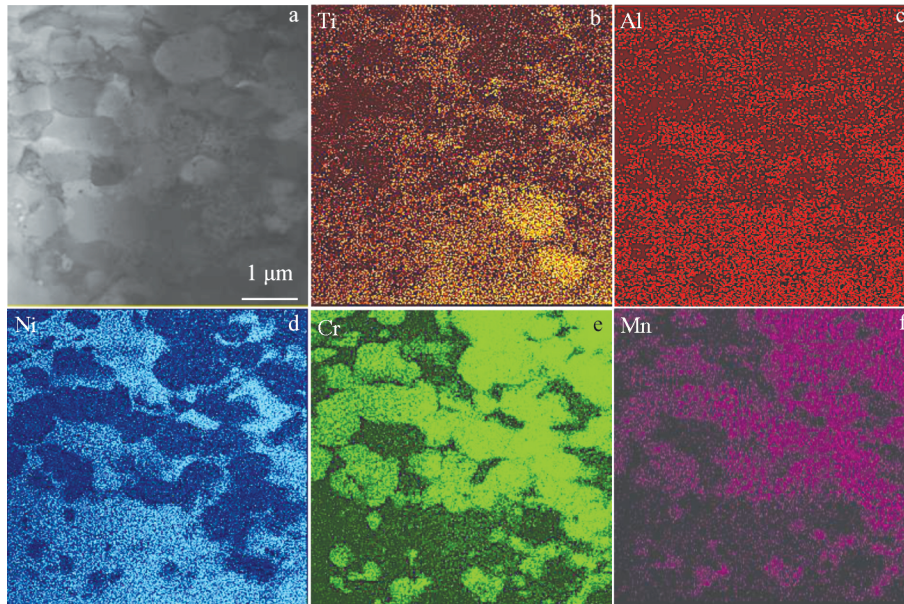


Fig.8 STEM image (a) and EDS mapping of Ti (b), Al (c), Ni (d), Cr (e), and Mn (f) element of IPZ

Near TMAZ of GH3039 alloy, because the Ni-rich grains attached to the existing grains grow, the Ni-rich grains are in vertically teeth-like shape. The Cr-rich grains are embedded in the Ni-rich grains. Away from the interface of about 0.4 μm, grains rich in Ni or Cr grow into large equiaxed grains. Therefore, the dynamic recrystallization occurs on both sides

The zone shown in Fig.8 corresponds to intermediate phase layer B in Fig.4. It can be seen that in IPZ, the distribution of elements Ni and Cr is complementary. The Cr-rich grains are spherical, meaning that they are formed by precipitation in the base material by the amplitude modulation, and the rest forms the Ni-rich grains. Also, it can be found that the regions rich in Ni coincide with those rich in Ti and Al, and the regions rich in Cr coincide with those of rich Mn, indicating that Ti and Al are easy to dissolve in the Ni-rich grains, i.e., Ti and Al have high solubility in Ni-rich grains. Meanwhile Mn belonging to the iron family with Cr is easily soluble in Cr-rich grains.

In order to determine the phase shown in Fig. 8, TEM observation with selected area electron diffraction (SAED) pattern was used. According to the results from element sur-

face scanning, the phase in the region rich in Cr was chosen (area marked by circle in Fig.9a), and related SAED pattern was obtained, as shown in Fig.9.

It can be confirmed that the SAED pattern in Fig. 9b is along zone axis [111], and the Cr-rich phase region is body-centered cubic α-Cr with lattice parameter $a=0.288$ nm and interplanar crystal spacing $d=0.2036$ nm.

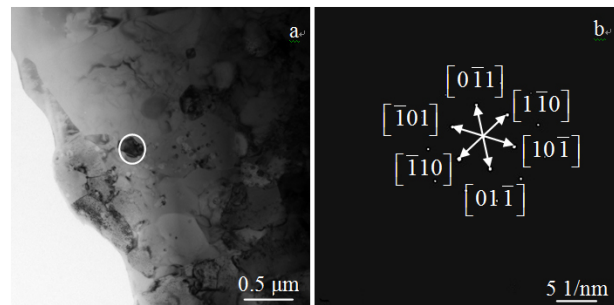


Fig.9 TEM image of welded zone (a) and SAED (area marked by circle) pattern along zone axis [111] (b)

Table 3 Element content and possible phases in different intermediate phase layers in TiAl/GH3039 friction welding joint (at%)

| Zone | Al | Cr | Ti | Fe | Mo | V | Ni | Possible phase |
|---------|-------|-------|-------|------|------|------|-------|----------------------------------------------------------|
| GH3039 | 0.08 | 23.49 | 0.17 | 1.71 | 1.22 | 0.00 | 71.68 | A |
| Layer A | 0.72 | 22.79 | 10.76 | 1.46 | 1.18 | 0.36 | 61.47 | (Ni, Cr) _{ss} |
| Layer B | 18.20 | 12.52 | 21.16 | 0.62 | 0.35 | 1.25 | 44.95 | $\tau_3 + \alpha\text{-Cr}$ |
| Layer C | 35.20 | 7.20 | 28.03 | 0.27 | 0.32 | 2.29 | 26.01 | $\tau_3\text{-Al}_{1+x-y}\text{Ti}_{1+y}\text{Ni}_{1-x}$ |
| Layer D | 35.52 | 3.87 | 52.84 | 0.04 | 0.24 | 2.98 | 4.31 | $\alpha_2 + \tau_3$ |
| TiAl | 46.87 | 1.04 | 49.62 | 0.00 | 0.00 | 2.47 | 0.00 | $\gamma\text{-TiAl} + \alpha_2\text{-Ti}_3\text{Al}$ |

In order to further determine the specific composition of each intermediate phase layer, EPMA was used to analyze the element distributions of each intermediate phase layer in Fig.4. The results are listed in Table 3. Based on EDS linear scanning and mapping analyses of WZ, the TEM results, and the binary and multicomponent phase diagrams of Ti, Al, Cr, and Ni, the possible intermediate phases of each layer are preliminarily determined, as listed in Table 3. The crystal structure of τ_3 -Al_{1+x}·Ti_{1+y}·Ni_{1-x} is hP12, and the lattice space group symbol is P6₃/mmc. The interface microstructure of the friction welding zone between γ -TiAl intermetallic and GH3039 alloy superalloy is γ -TiAl+ α_2 -Ti₃Al/ α_2 + τ_3 / τ_3 -Al_{1+x}·Ti_{1+y}·Ni_{1-x}/ τ_3 + α -Cr/(Ni, Cr)_{ss}/GH3039.

3 Conclusions

1) The γ -TiAl intermetallic and GH3039 superalloy can be friction welded, and the maximum tensile strength of the weld joint is more than 400 MPa.

2) Due to thermo-mechanical coupling during friction welding, the plastic deformation of thermo-mechanically affected zone (TMAZ) on GH3039 side is much more obvious than that on TiAl side, and dynamic recrystallization occurs on both sides.

3) There are four continuous intermediate phase layers formed at intermediate phase zone (IPZ). Weld zone (WZ) includes IPZ and element diffusion zone on both sides.

4) In WZ near GH3039 side, the distribution of Ni-rich and Cr-rich grains is complementary. Ti and Al are easily soluble in the Ni-rich crystal grains, and Mn is easily soluble in the Cr-rich crystal grains.

5) A large number of Cr-rich grains formed in the bonding zone are body-centered cubic α -Cr with lattice constant $a=0.288$ nm and interfacial spacing $d=0.2036$ nm.

References

- Du Suigeng, Fu Li, Wang Jinwei et al. *The Chinese Journal of Nonferrous Metals*[J], 2003, 13(2): 323 (in Chinese)
- Albert B, Völkl R, Glatzel U. *Metallurgical and Materials Transactions A*[J], 2014, 45(10): 4561
- Shi Zhaoxia, Dong Jianxin, Zhang Maicang et al. *Journal of Alloys and Compounds*[J], 2013, 571: 168
- Wu Xinhua. *Intermetallics*[J], 2006, 14(10): 1114
- Su Yanqing, Liu Tong, Li Xinzong et al. *Acta Metallurgica Sinica*[J], 2018, 54(5): 647 (in Chinese)
- Noda T, Shimizu T, Okabe M et al. *Materials Science and Engineering A*[J], 1997, 239-240: 613
- Shiue R K, Wu S K, Chen S Y. *Intermetallics*[J], 2004, 12(7): 929
- Li Haixin, Wei Hongmei, He Peng et al. *Intermetallics*[J], 2013, 34: 69
- Dong Honggang, Yang Zhonglin, Wang Zengrui et al. *Journal of Materials Science & Technology*[J], 2015, 31(2): 217
- Niu G B, Wang D P, Yang Z W et al. *Ceramics International*[J], 2017, 43(1): 439
- Hauschildt K, Stark A, Schell N et al. *Intermetallics*[J], 2019, 106: 48
- Li Yulong, He Peng, Feng Jicai. *Scripta Materialia*[J], 2006, 55(2): 171
- Sequeiros E, Guedes A, Pinto A et al. *Materials Science Forum* [J], 2012, 730-732: 835
- Ding J, Wang J N, Hu Z H et al. *Materials Science and Technology*[J], 2002, 18(8): 908
- Guoqing C, Binggang Z, Wei L et al. *Intermetallics*[J], 2011, 19(12): 1857
- Li Yuxuan, Wang Houqin, Han Ke et al. *Journal of Materials Processing Technology*[J], 2017, 250: 401
- Ustinov A I, Falchenko Y V, Ishchenko A Y et al. *Intermetallics* [J], 2008, 16(8): 1043
- Simões S, Viana F, Ramos A S et al. *Materials Chemistry and Physics*[J], 2016, 171: 73
- Zhao Kun, Liu Yong, Huang Lan et al. *Journal of Materials Processing Technology*[J], 2016, 230: 272
- Du Zhihao, Zhang Kaifeng, Lu Zhen et al. *Vacuum*[J], 2018, 150: 96
- Cai Xiaolong, Sun Daqian, Li Hongmei et al. *Optics & Laser Technology*[J], 2017, 97: 242
- Cai Xiaolong, Sun Daqian, Li Hongmei et al. *Optics & Laser Technology*[J], 2019, 111: 205
- Miyashita T, Hino H. *Journal of the Japan Institute of Metals*[J], 1994, 58(2): 215
- Lee W B, Kim M G, Koo J M et al. *Journal of Materials Science* [J], 2004, 39(3): 1125
- Lee W B, Kim Y J, Jung S B. *Intermetallics*[J], 2004, 12(6): 671
- Dong H G, Yu L Z, Gao H M et al. *Transactions of Nonferrous Metals Society of China*[J], 2014, 24(10): 3126
- Dong H G, Yu L Z, Deng D et al. *Materials and Manufacturing Processes*[J], 2015, 30(9): 1104
- Kumar R, Balasubramanian M. *Defence Technology*[J], 2015, 11(1): 65
- Du Suigeng, Wang Songlin, Xu Wanting. *Materials*[J], 2020, 13(9): 2072

TiAl 合金与 GH3039 摩擦焊接界面组织

杜随更¹, 李 娜^{1,2}, 王松林¹

(1. 西北工业大学 航空发动机高性能制造工业和信息化部重点实验室, 陕西 西安 710072)

(2. 平凉职业技术学院 机电工程系, 甘肃 平凉 744000)

摘 要: 使用 GH3039 合金作为 γ -TiAl 与碳钢摩擦焊接的过渡第三体, 采用扫描电子显微镜 (SEM) 和透射电子显微镜 (TEM) 分析了 TiAl/GH3039 摩擦焊接接头的界面结构。结果表明, γ -TiAl 和 GH3039 摩擦焊接接头的最大抗拉伸强度能达到 400 MPa 以上。GH3039 一侧热力影响区的塑性变形大于 TiAl 一侧, 并且在两侧均发生动态再结晶。接近 GH3039 母材相层中的 Ni 含量几乎不变, 接近 TiAl 母材相层中的 Ti 含量也几乎不变。在 GH3039 侧面附近的焊接区中, 富 Ni 和富 Cr 晶粒的分布是互补的。Ti 和 Al 容易溶于富 Ni 的晶粒中, 而 Mn 容易溶于富 Cr 的晶粒中。在结合区中形成的大量富 Cr 晶粒是体心立方结构的 α -Cr。 γ -TiAl 和 GH3039 摩擦焊接的典型界面结构为: γ -TiAl+ α_2 -Ti₃Al/ α_2 + τ_3 -Al_{1+x-y}Ti_{1+y}Ni_{1-x}/ τ_3 + α -Cr/(Ni, Cr)_{ss}/GH3039。

关键词: 摩擦焊接; TiAl 金属间化合物; GH3039 高温合金; 连接机理; 界面结构

作者简介: 杜随更, 男, 1963 年生, 博士, 教授, 西北工业大学航空发动机高性能制造工业和信息化部重点实验室, 陕西 西安 710072, 电话: 029-88495264, E-mail: fwcenter@nwpu.edu.cn